REPRESENTING IMAGES IN 200 BYTES: COMPRESSION VIA TRIANGULATION

David Marwood, Pascal Massimino, Michele Covell, Shumeet Baluja

Google, Inc

ABSTRACT

A rapidly increasing portion of internet traffic is dominated by requests from mobile devices with limited and metered bandwidth constraints. To satisfy these requests, it has become standard practice for websites to transmit small and extremely compressed image previews as part of the initial page load process to improve responsiveness. Increasing thumbnail compression beyond the capabilities of existing codecs is therefore an active research direction. In this work, we concentrate on extreme compression rates, where the size of the image is typically 200 bytes or less. First, we propose a novel approach for image compression that, unlike commonly used methods, does not rely on block-based statistics. We use an approach based on an adaptive triangulation of the target image, devoting more triangles to high entropy regions of the image. Second, we present a novel algorithm for encoding the triangles. The results show favorable statistics, in terms of PSNR and SSIM, over both the JPEG and the WebP standards.

Index Terms— Compression, Triangulation, Thumbnails

1. INTRODUCTION

The need for highly compressed images continues to increase. A rapidly increasing portion of internet traffic is dominated by requests from mobile devices with limited and often metered bandwidth constraints. Efficient delivery of quality thumbnails is an active area of interest to some of the largest Internet companies, including Google [1], Facebook [2] and Apple [3]. In addition to decreased download latency and bandwidth for end users, reducing image size also helps with storage requirements for billions of thumbnails that need to be rapidly accessed.

JPEG has long been a standard approach for image compression. In this study, we examine compression in an operating regime where JPEG and other popular approaches do not fare well: under 200 bytes. Usually, when extreme compression is required, it is addressed with domain specific techniques, specialized for faces [4], satellite imagery [5], smooth synthetic images [6], and surveillance [7], among others.

A powerful, recent, image compression approach is *WebP*. Per [1], WebP lossless images are 26% smaller in size compared to PNGs. WebP lossy images are 25-34% smaller than comparable JPEG images at an equivalent SSIM quality index. This is the standard to which we will compare.

The basis of many of the popular compression techniques is a subdivision of the image into a set of blocks. Our approach, which is based on triangulation, does not use a block approach nor a predefined, or uniform, spacing of triangles over the image. Instead, we use a limited set of vertices which are assigned a color index from a small colormap; simple color interpolation between each of the triangle vertices is used to fill in the triangles to create the resultant image. More triangles are devoted to the complex (high entropy) regions. Triangulation has previously been used in a diverse set of approaches for compression, see [8, 9, 10]. Finally, other experimental compression approaches use deep neural networks [11, 12] and diffusion [13, 14].

2. TRIANGULATION OF IMAGES

There are two broad components of our approach. The first is creating an effective triangulation and the second is efficiently encoding the triangulation. The triangulation component can be thought of as two pieces that must interact well: selecting where to place the triangulation's vertices and assigning a single color to each vertex. For transmission efficiency, we would like to minimize the number of vertices and the total number of unique colors. Rather than transmitting the connectivity matrix, we consider only Delaunay Triangulations that can be constructed in both the encoding and decoding stages given only the vertex coordinates. See also [15, 16].

Our approach follows a generate-and-test paradigm. We begin with a small thumbnail image, I (usually 221×221). In the simplest version of our algorithm, shown in Figure 1, we begin with an over-complete set of vertices on a fixed-size grid and prune them to a smaller set until the set and the color information can fit in 200 bytes. The grid-size is our only parameter for adjusting the compression rate.

Using only this simple procedure, the final triangulations and resulting images are shown in Figure 2. The most salient observation is that the triangles cluster around the higher entropy regions. Homogeneous regions such as the sky have fewer triangles. Quantitatively, PSNR quality was close to WebP, but did not consistently out-perform WebP. Understanding the deficiencies is key to understanding the design of our improved approach. (1) The colors, based on global

1. *Insert initial, evenly-spaced candidate coordinate points from a subsampled version of I, into a set P.* By considering only a fixed subset P of pixels locations for triangle coordinates, the encoding is faster and more compressible.
2. *Select a set C of colors.* Cluster the colors in I and select the 8 to 16 representative ones. Each vertex $p \in P$ is assigned a color in C.
3. *Triangulate.* Given P, create a Delaunay Triangulation.
4. *Generate I' and test.* With C and P, the triangles are filled using bilinear interpolation, yielding image I'. The difference between I and I' is tested with either SSIM or PSNR.
5. *Find least important vertex $p_x \in P$.* For each $p \in P$, in turn, remove that p, re-triangulate and fill triangles to create I''. Set p_x to the point that produces the lowest error.
6. *Remove least important vertex, p_x.* Continue from 5.

Fig. 1: Baseline: A Deterministic, Greedy, Approach.

image characteristics, are selected once and never adapted. (2) The only allowed change is to remove vertices: they are never added back or moved slightly to find a better combinations of triangles. (3) The Baseline makes a greedy choice for every proposed mutation, limiting the effectiveness of local search once regions of high performance are found.

To address the difficulties, we turn to a stochastic variant. An often-used technique to search discrete, non-differentiable, optimization landscapes is with randomized search heuristics such as hill climbing [17], evolutionary algorithms and strategies [18, 19] and simulated annealing [20].

A stochastic hill climbing variant of the Baseline is given in Figure 3. At the expense of determinism, this allows us to more thoroughly explore the search space and adapt color settings. There are six possible operations other than the single "remove vertex" operator that the Baseline variant employed.

original   8 color   triangulated   result
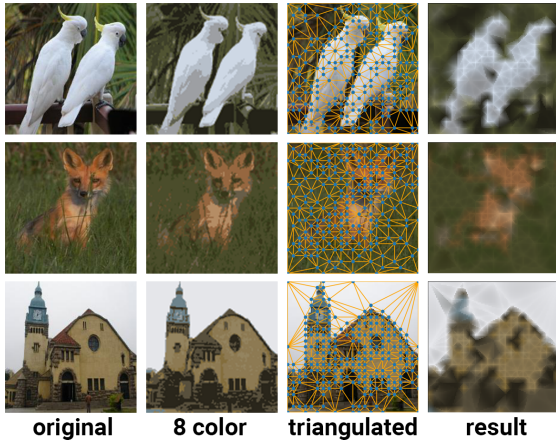
Fig. 2: Results for baseline. From left: Original Image, 8 colors version, triangulation, and result. Note that the triangulation places more triangles in higher entropy regions.

1. *Initialize P.* Greedily select P as a set of 300 vertices that minimizes the difference with the input image.
2. *Initialize C.* Agglomerate the individual vertex colors down to 8 colors in the color table C.
3. *Initialize vertex colors.* For each vertex, assign the color index in C closest to the vertex's color in the input image.
4. *Triangulate.* Given P, create a Delaunay triangulation.
5. *Mutate.* A mutation is a subset of the actions below. An action is included (once) with some probability.
   (a) *Displace a vertex.* Move a vertex either horizontally or vertically one grid point.
   (b) *Add a random vertex.*
   (c) *Remove a random vertex.*
   (d) *Re-assign vertex color randomly.*
   (e) *Add a color to C and re-assign vertex colors.*
   (f) *Remove a color from C and re-assign vertex colors.*
   (g) *Perturb a color entry.* Select a color entry and a channel and randomly change by ± 1.
6. *Re-triangulate and retain the mutation if it improved the trade-off between error and size. Otherwise discard the mutation.* Repeat from Step 5.

Fig. 3: A Stochastic Approach.

Note that 4 of 7 mutation operators (Steps 5(d)-(g) in Figure 3) modify colors; no color modification was employed in the Baseline. Second, vertices can be added (even if they had been previously removed) if they are found to improve the score; vertices can also make "localized" moves to nearby grid points. Third, instead of always removing vertices until the desired byte-size was reached, the acceptance of a move is based on whether that move improves the quality-vs-size objective function.
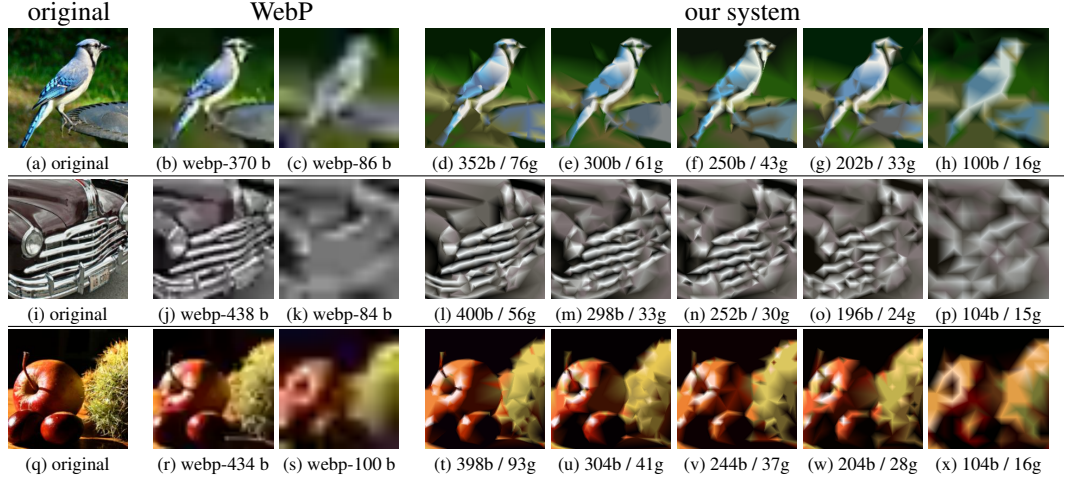
In contrast to the Baseline, the stochastic variant is initialized with only a small set of vertices P. As before, they are all on a pre-specified grid. The search progresses by *mutating* the current solution set and evaluating the result with respect to the quality-vs-size objective function.

2.1. Encoding the Triangulation

Once we have selected a triangulation, we need to losslessly compress that representation. In all cases discussed below, we use asymmetric numerical systems (ANS) [21] which is a computationally efficient method to achieve the compression rates of arithmetic encoding [22].

We send a "header" containing basic parameters such as the grid size, the number of vertices, and the color table. The color-table entries are sorted by frequency of use (starting with the most common). The color table is then coded by giving the number of colors, the color channel values (quantized to 6 bits per YCoCg channel), and the usage frequencies

Fig. 4: Visualizing the results vs. image byte size. For each of the 3 original images (left most column), the image at 2 WebP (roughly 400, 100 bytes) and 5 compression levels for our system (roughly 400, 300, 250, 200, 100) are given. Byte size (b) and grid size (g) given for each result from our system.

original   WebP   our system

(a) original   (b) webp-370 b   (c) webp-86 b   (d) 352b / 76g   (e) 300b / 61g   (f) 250b / 43g   (g) 202b / 33g   (h) 100b / 16g

(i) original   (j) webp-438 b   (k) webp-84 b   (l) 400b / 56g   (m) 298b / 33g   (n) 252b / 30g   (o) 196b / 24g   (p) 104b / 15g

(q) original   (r) webp-434 b   (s) webp-100 b   (t) 398b / 93g   (u) 304b / 41g   (v) 244b / 37g   (w) 204b / 28g   (x) 104b / 16g

for each of the entries. We code the color channel values as a correction from the average of the previously transmitted values for that channel (e.g., the Y channel), with the first entry's prediction set to the mid-point gray. The histogram table for these color differences are sent as part of the header.

The color-entry frequencies are transmitted using a binomial distribution model: we use a "fair selection" model on the remaining colors and vertices (i.e., $N = V_{C_r}$ trials, where V_{C_r} is the number of remaining vertices not counted by the previous color entries, and a success probability of $p = 1/|C_r|$ where $|C_r|$ is the number of remaining color-table entries, C_r). We improve on this probability model by limiting the considered values of the distribution to be at least $V_{C_r}/|C_r|$ (based on knowing that the *upcoming* entries have been sorted) and at most the frequency count of the previous entry (based on knowing that the *previous* and *current* entries have been sorted). Using this approach to color-entry frequency coding, we save 1%-3% of the file size, on average, compared with using a simple uniform-probability model of the distributions.

We also explore alternative approaches to compressing the vertex locations and their color assignments. For the vertex locations, the simplest alternative is to send one bit (without arithmetic coding) per grid point to mark whether it is used as a vertex. This takes N_g bits, where N_g is the number of grid points and corresponds to using a 0.5 probability of occupancy. We can do better by using a fixed, but more accurate, probability of occupancy: V_t/N_g where V_t is the total number of vertices (sent in the header). In our experiments, this fixed-probability only saved an average of 1% of the single-bit-per-grid-point approach. We also tried using run-length codes (coding the run length of "unoccupied" grid points between vertices), however the overhead of sending the distribution of run-lengths made this approach worse.

The best compression in our tests uses an adaptive-probability approach to compressing the occupancy map. In this approach, we simply update our probability model as we progress through the grid, so that at each point the model

probability is V_r/N_r where V_r and N_r are the remaining vertex and grid point counts, respectively. In our tests, this gave a savings of 2.25% over the single-bit-per-grid-point approach.

We use a similar approach for coding the color-table index for each vertex. Since we know the color-entry frequencies, we can use adaptive models for these indices. Instead of simply using these remaining-count probabilities, we can explicitly treat the color index coding as a chain of Boolean encodings — each with the probability indicated by the remaining-count probability for the corresponding color-table entry but with their order of encoding set by a spatially adaptive prediction. This helps even without changing any of the model probabilities because once we see a "true" Boolean value, we can stop encoding for that vertex and move to the next one. We determine the order of encoding by sorting the previously seen (and already transmitted) colors based on their Manhattan distance to the current vertex, with ties broken in favor of the more probable color. Using this ordering results in a $1\% - 3\%$ file size reduction for the color-table frequencies. Using the spatially-adaptive ordering provides an additional 0.66% file-size reduction.

3. EXPERIMENTS

In this section, we present a summary of the experiments we performed. The performance is assessed with *PSNR* (Peak-Signal-to-Noise Ratio) and *SSIM* (Structural Similarity Index) [23], which is based on the visible structures in the image, and is considered a perceptual metric. All of the results reported are the average of compressing 1,024 images, each consisting of 221×221 pixels. The images were randomly selected from the ImageNet training set [24]. Figure 4 shows the effects of final byte-size on the results obtained by the stochastic variant described in the previous section. The larger the allowed byte-size, the finer the initial grid can be. Our results are shown for grid sizes from 15×15 (around 100 bytes, compressed) up to 96×96 (around 400 bytes).
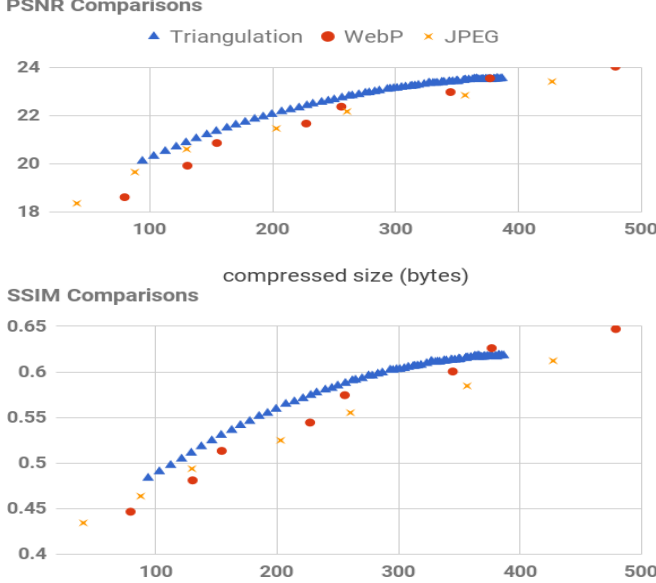
Fig. 5: Measuring quality as a function of bytes. WebP becomes competitive at approximately 400 bytes, JPEG is competitive after 500 (not shown).

Quantitative results are shown in Figure 5. When measured with either metric, PSNR or SSIM, the triangulation approach outperforms both WebP and JPEG. As can be seen, JPEG performs quite poorly in this operating range. Also note that to be as favorable to JPEG as possible, we set quality=20, which produced the best quality/size, and used headerless JPEG encoding. Adding a header significantly deteriorates performance. WebP is a close competitor at quality=10. At the range of interest (200 bytes) we outperform WebP in both metrics. By 400 bytes, WebP and the triangulation approach perform equally. Beyond 400 bytes, we again expect WebP to have an advantage.

Despite the promising results in Figure 5, we need to ensure that the average performance is indicative of expected performance. In Figure 6, we provide histograms of the PSNR and SSIM errors on the 1,024 image test set. In the same figure, we also look at the best and worst performing examples: intuitively, the worst cases have large entropy regions (similar to checkerboard patterns) while the best ones have large areas of similar colors.

Finally, we would like to give a better understanding at the best steps in our pipeline. In the interest of space, we present one graph in Figure 7 that provides the most insight into the benefits of the stochastic approach over the baseline. We repeat all of our experiments using only a subset of the operators described in Figure 3 Step 5. The biggest improvement is from vertex modfication and, next, from color-entry perturbation (PSNR shown, same for SSIM). The gains seen with color modification suggest that pre-computing the color table based on the color clusters in the thumbnail is not adequate for use in a triangulated approximation.
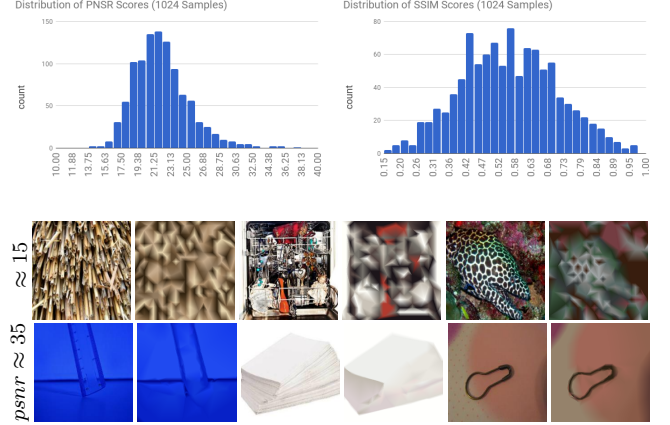
Fig. 6: Histogram of Results (at bytes=200). Top Left: PSNR, Top Right: SSIM. 3 Cases with poor (middle row) and high PSNR (last row). Shown alternating: original, compressed.

4. CONCLUSIONS & FUTURE WORK

We have presented an approach to compressing images to extremely small byte sizes. In the operating range of interest, 200-400 bytes, standard JPEG operates poorly. With tiny thumbnails under 400 bytes, we surpass the latest deployed version WebP, version 1.0.0, in both PSNR and SSIM. Only after ∼400 bytes, does WebP do better. Further, our representation is scale-free: the triangles can be easily scaled and simply rendered with low-level primitives.

There are three immediate avenues for future work. The first is the large-scale human evaluation of the images to verify the SSIM and PSNR improvements. Second, the stochastic search process can be computationally expensive; domain-specific heuristics to narrow the search space may help. Third, we have found that adding synthetic noise in post-processing can enhance the perceived quality without always improving the quality/size score. Further research on a perceptual metric dedicated to thumbnails is needed.
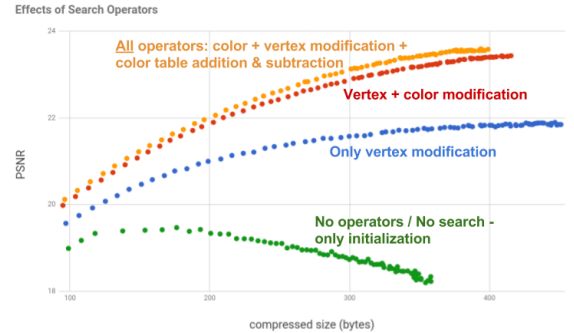
Fig. 7: What makes the algorithm (Figure 3) work? Green: no search, only initialization. Blue: using only vertex-modification operators (steps 5 (a)-(c)). Red: adding color perturbation (steps 5 (a)-(c) plus (d) and (g)). Yellow: all operators (steps 5 (a)-(g)).

5. REFERENCES

[1] Google Developers, "A new image format for the web," https://developers.google.com/speed/webp/, 2016.

[2] B.K. Cabral and E. Kandrot, "The technology behind preview photos," https://code.facebook.com/posts/991252547593574/the-technology-behind-preview-photos/, 2015.

[3] Apple Inc., "Using HEIF or HEVC media on Apple devices," https://support.apple.com/en-us/HT207022, 2017.

[4] Ori Bryt and Michael Elad, "Compression of facial images using the K-SVD algorithm," *Journal of Visual Communication and Image Representation*, vol. 19, no. 4, pp. 270–282, 2008.

[5] Bormin Huang, *Satellite data compression*, Springer Science & Business Media, 2011.

[6] Alexandrina Orzan, Adrien Bousseau, Pascal Barla, Holger Winnemöller, Joëlle Thollot, and David Salesin, "Diffusion curves: a vector representation for smooth-shaded images," *Communications of the ACM*, vol. 56, no. 7, pp. 101–108, 2013.

[7] Jing-Ya Zhu, Zhong-Yuan Wang, Rui Zhong, and Shen-Ming Qu, "Dictionary based surveillance image compression," *Journal of Visual Communication and Image Representation*, vol. 31, pp. 225–230, 2015.

[8] Sébastien Bougleux, Gabriel Peyré, and Laurent D Cohen, "Image compression with anisotropic triangulations," in *Computer Vision, 2009 IEEE 12th International Conference on*. IEEE, 2009, pp. 2343–2348.

[9] Franck Davoine, Marc Antonini, J-M Chassery, and Michel Barlaud, "Fractal image compression based on delaunay triangulation and vector quantization," *IEEE Transactions on Image Processing*, vol. 5, no. 2, pp. 338–346, 1996.

[10] Laurent Demaret, Nira Dyn, and Armin Iske, "Image compression by linear splines over adaptive triangulations," *Signal Processing*, vol. 86, no. 7, pp. 1604–1616, 2006.

[11] J Jiang, "Image compression with neural networks–a survey," *Signal Processing: Image Communication*, vol. 14, no. 9, pp. 737–760, 1999.

[12] George Toderici, Sean M. O'Malley, Sung Jin Hwang, Damien Vincent, David Minnen, Shumeet Baluja, Michele Covell, and Rahul Sukthankar, "Variable rate image compression with recurrent neural networks," in *International Conference on Learning Representations*, 2016.

[13] Christian Schmaltz, Joachim Weickert, and Andrés Bruhn, "Beating the quality of jpeg 2000 with anisotropic diffusion," in *Pattern Recognition*, Joachim Denzler, Gunther Notni, and Herbert Süße, Eds., Berlin, Heidelberg, 2009, pp. 452–461, Springer Berlin Heidelberg.

[14] Laurent Hoeltgen, Pascal Peter, and Michael Breuß, "Clustering-based quantisation for pde-based image compression," *Signal, Image and Video Processing*, vol. 12, no. 3, pp. 411–419, Mar 2018.

[15] Hana Galperin and Avi Wigderson, "Succinct representations of graphs," *Information and Control*, vol. 56, no. 3, pp. 183–198, 1983.

[16] György Turán, "On the succinct representation of graphs," *Discrete Applied Mathematics*, vol. 8, no. 3, pp. 289–294, 1984.

[17] Heinz Mühlenbein, "How genetic algorithms really work: Mutation and hillclimbing.," in *Parallel Problem Solving from Nature*, 1992, vol. 92, pp. 15–25.

[18] Dipankar Dasgupta and Zbigniew Michalewicz, *Evolutionary algorithms in engineering applications*, Springer Science & Business Media, 2013.

[19] T. Salimans, J. Ho, X. Chen, S. Sidor, and I. Sutskever, "Evolution Strategies as a Scalable Alternative to Reinforcement Learning," *ArXiv e-prints*, Mar. 2017.

[20] Scott Kirkpatrick, C Daniel Gelatt, Mario P Vecchi, et al., "Optimization by simulated annealing," *Science*, vol. 220, no. 4598, pp. 671–680, 1983.

[21] J. Duda, K. Tahboub, N. J. Gadgil, and E. J. Delp, "The use of asymmetric numeral systems as an accurate replacement for huffman coding," in *2015 Picture Coding Symposium (PCS)*, May 2015, pp. 65–69.

[22] David J.C. MacKay, *Information Theory, Inference, and Learning Algorithms*, chapter 6 Stream Codes, Cambridge University Press, Cambridge, 2003.

[23] Zhou Wang, Alan C Bovik, Hamid R Sheikh, and Eero P Simoncelli, "Image quality assessment: from error visibility to structural similarity," *IEEE transactions on image processing*, vol. 13, no. 4, pp. 600–612, 2004.

[24] Olga Russakovsky, Jia Deng, Hao Su, Jonathan Krause, Sanjeev Satheesh, Sean Ma, Zhiheng Huang, Andrej Karpathy, Aditya Khosla, Michael S. Bernstein, Alexander C. Berg, and Fei-Fei Li, "Imagenet large scale visual recognition challenge," *International Journal of Computer Vision*, vol. 115, no. 3, pp. 211–252, 2015.

Supplemental Materials

The below are seven example images, which we have taken from our evaluation set. The subsequent pages show them encoded with different sized grids, across our full range of bitrates. Below each image, we list PSNR, SSIM, and file size. We use file size, instead of BPP, since our triangle representation does not limit the reconstruction to any fixed size. The reconstructions are shown at 221×221, but larger-sized reconstructions will retain the sharpness of these reconstructions, since the upsampling conversion is done before the interpolation, used to fill in the Delaney triangles. The ridges that are seen in the 221×221 reconstructions will remain as sharp, even at larger image sizes, due to the vertex-based representation.

Original target images

PSNR: 20.18; SSIM: 0.515; bytes: 98.0

PSNR: 20.43; SSIM: 0.531; bytes: 128.0

PSNR: 21.15; SSIM: 0.550; bytes: 152.0

PSNR: 21.43; SSIM: 0.565; bytes: 176.0

PSNR: 21.76; SSIM: 0.578; bytes: 208.0

PSNR: 22.06; SSIM: 0.590; bytes: 236.0

PSNR: 22.48; SSIM: 0.609; bytes: 256.0

PSNR: 22.63; SSIM: 0.617; bytes: 278.0

PSNR: 22.66; SSIM: 0.622; bytes: 298.0

PSNR: 22.73; SSIM: 0.624; bytes: 314.0

PSNR: 22.86; SSIM: 0.635; bytes: 344.0

PSNR: 23.20; SSIM: 0.643; bytes: 370.0
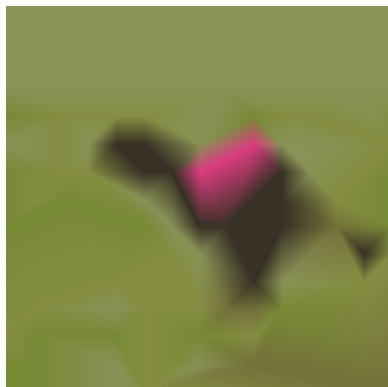
PSNR: 24.31; SSIM: 0.578; bytes: 70.0
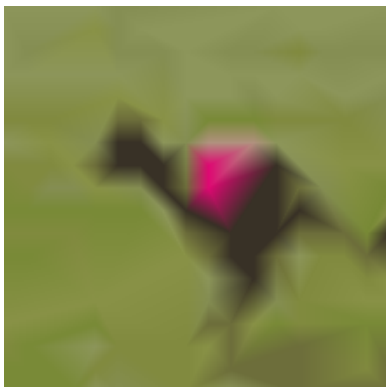
PSNR: 24.80; SSIM: 0.586; bytes: 120.0

PSNR: 25.14; SSIM: 0.594; bytes: 140.0

PSNR: 25.28; SSIM: 0.604; bytes: 168.0

PSNR: 26.11; SSIM: 0.617; bytes: 192.0

PSNR: 26.52; SSIM: 0.635; bytes: 222.0
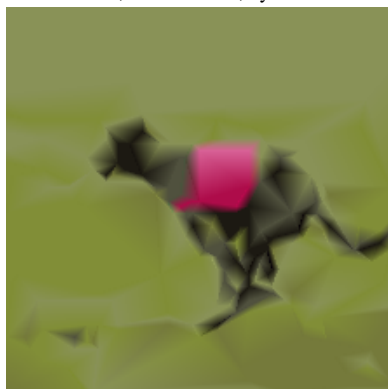
PSNR: 27.24; SSIM: 0.648; bytes: 246.0

PSNR: 26.97; SSIM: 0.643; bytes: 264.0
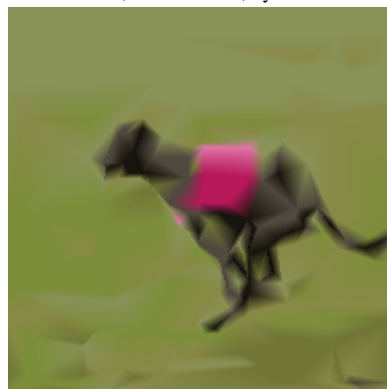
PSNR: 27.38; SSIM: 0.654; bytes: 288.0

PSNR: 27.03; SSIM: 0.649; bytes: 312.0

PSNR: 27.57; SSIM: 0.660; bytes: 340.0

PSNR: 27.20; SSIM: 0.659; bytes: 352.0

PSNR: 18.61; SSIM: 0.410; bytes: 96.0

PSNR: 18.97; SSIM: 0.422; bytes: 116.0

PSNR: 19.64; SSIM: 0.453; bytes: 154.0
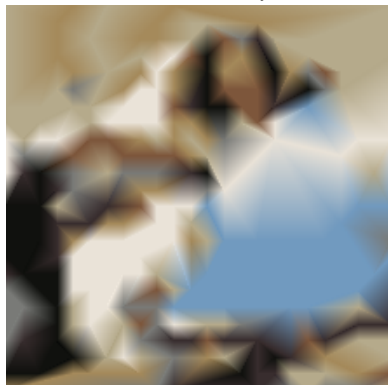
PSNR: 19.72; SSIM: 0.454; bytes: 178.0
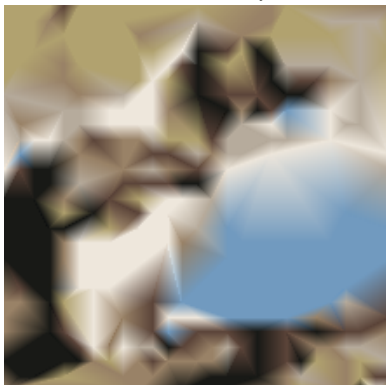
PSNR: 20.08; SSIM: 0.483; bytes: 194.0
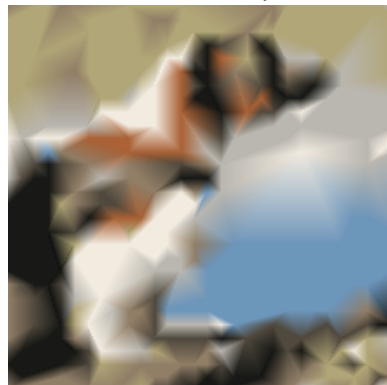
PSNR: 20.36; SSIM: 0.479; bytes: 230.0
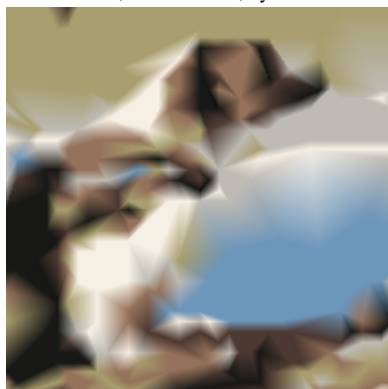
PSNR: 20.72; SSIM: 0.508; bytes: 268.0
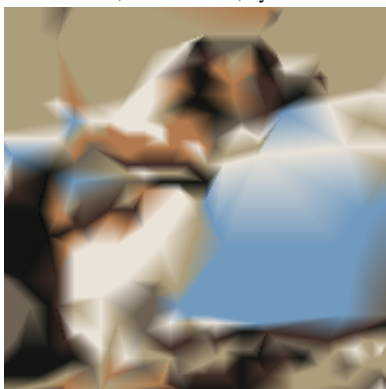
PSNR: 20.80; SSIM: 0.517; bytes: 286.0
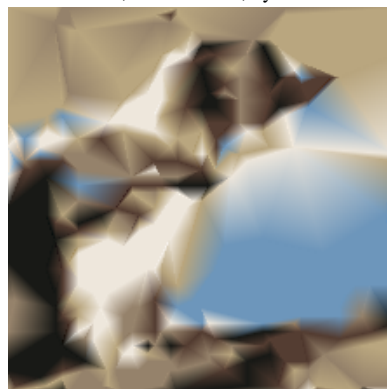
PSNR: 20.72; SSIM: 0.514; bytes: 302.0
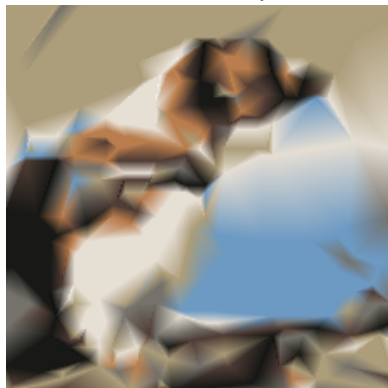
PSNR: 20.91; SSIM: 0.520; bytes: 328.0
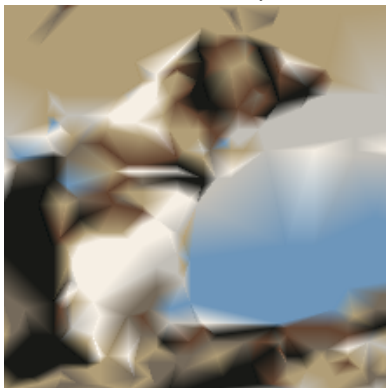
PSNR: 21.15; SSIM: 0.532; bytes: 344.0
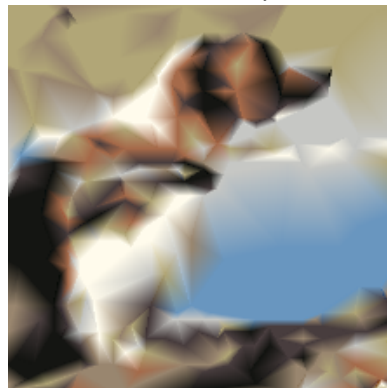
PSNR: 21.39; SSIM: 0.532; bytes: 374.0

PSNR: 26.22; SSIM: 0.625; bytes: 86.0

PSNR: 26.59; SSIM: 0.635; bytes: 118.0

PSNR: 27.36; SSIM: 0.648; bytes: 140.0

PSNR: 27.48; SSIM: 0.662; bytes: 164.0

PSNR: 27.91; SSIM: 0.666; bytes: 204.0
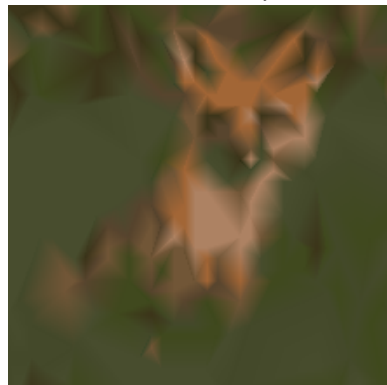
PSNR: 28.27; SSIM: 0.675; bytes: 248.0
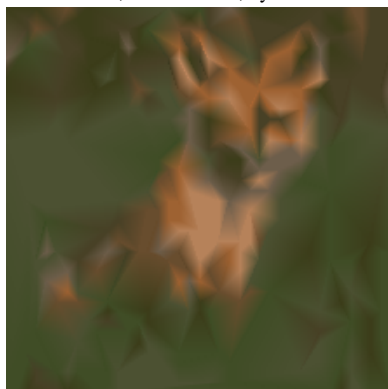
PSNR: 28.50; SSIM: 0.682; bytes: 282.0

PSNR: 28.78; SSIM: 0.689; bytes: 308.0
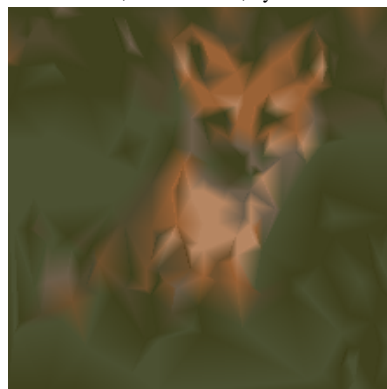
PSNR: 28.79; SSIM: 0.691; bytes: 336.0

PSNR: 28.77; SSIM: 0.689; bytes: 354.0

PSNR: 28.76; SSIM: 0.693; bytes: 370.0

PSNR: 29.04; SSIM: 0.701; bytes: 382.0
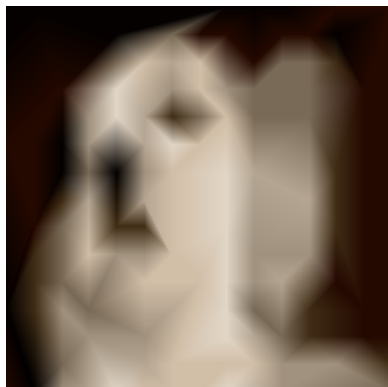
PSNR: 23.50; SSIM: 0.623; bytes: 94.0
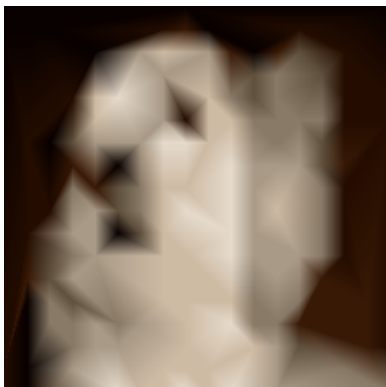
PSNR: 24.15; SSIM: 0.653; bytes: 116.0

PSNR: 24.95; SSIM: 0.670; bytes: 134.0
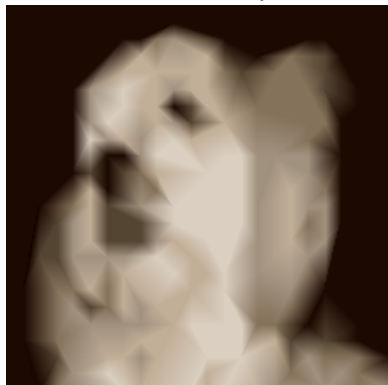
PSNR: 25.26; SSIM: 0.683; bytes: 146.0
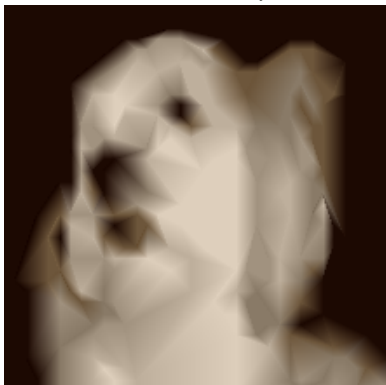
PSNR: 26.18; SSIM: 0.709; bytes: 198.0
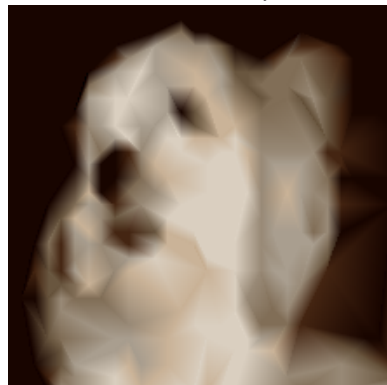
PSNR: 26.35; SSIM: 0.707; bytes: 208.0
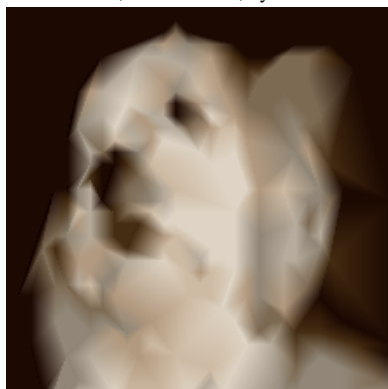
PSNR: 26.38; SSIM: 0.702; bytes: 216.0
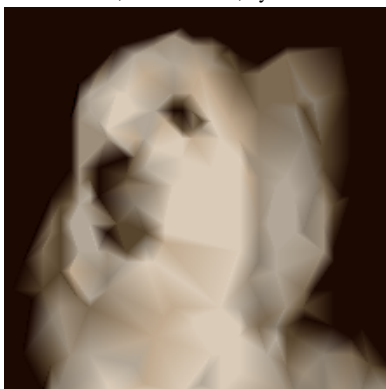
PSNR: 26.47; SSIM: 0.712; bytes: 238.0
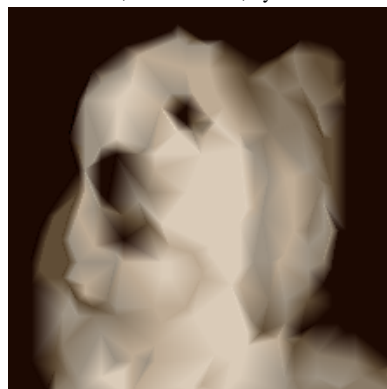
PSNR: 26.59; SSIM: 0.721; bytes: 258.0
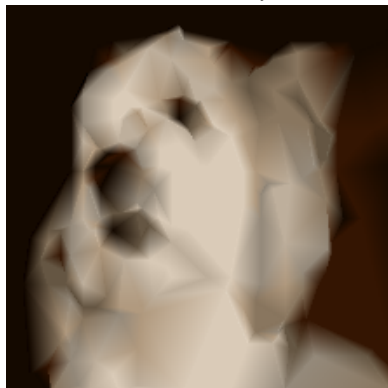
PSNR: 27.13; SSIM: 0.735; bytes: 288.0

PSNR: 27.60; SSIM: 0.749; bytes: 332.0
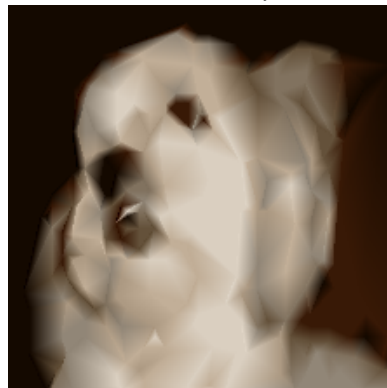
PSNR: 27.78; SSIM: 0.748; bytes: 342.0
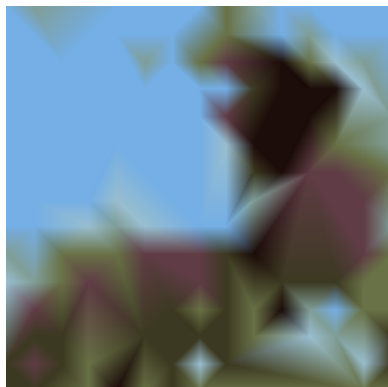
PSNR: 18.42; SSIM: 0.494; bytes: 90.0
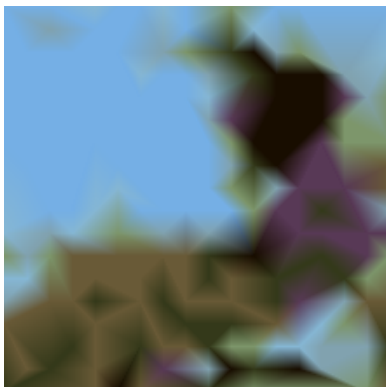
PSNR: 18.74; SSIM: 0.503; bytes: 124.0

PSNR: 19.08; SSIM: 0.524; bytes: 152.0

PSNR: 19.19; SSIM: 0.531; bytes: 170.0

PSNR: 19.56; SSIM: 0.546; bytes: 204.0

PSNR: 19.90; SSIM: 0.564; bytes: 252.0
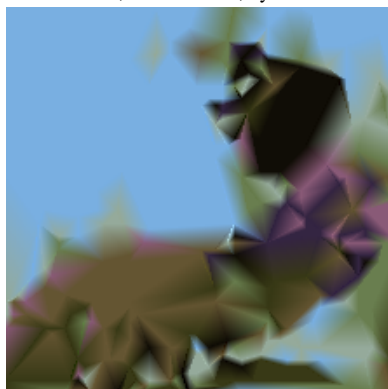
PSNR: 20.09; SSIM: 0.574; bytes: 312.0
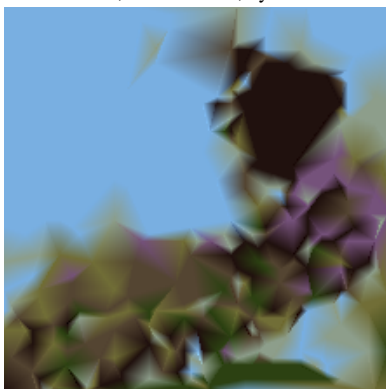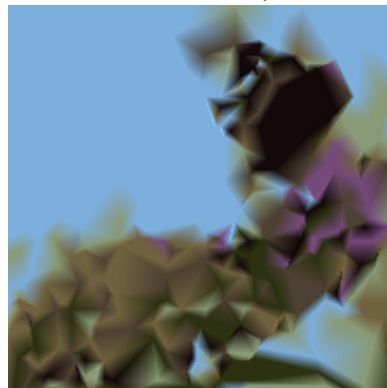

PSNR: 20.18; SSIM: 0.586; bytes: 336.0
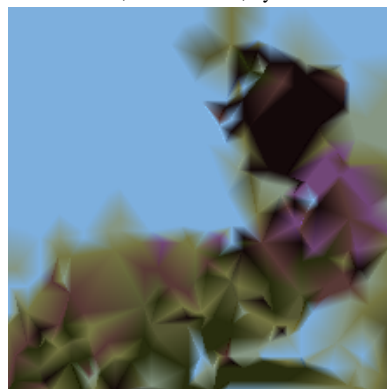
PSNR: 20.27; SSIM: 0.593; bytes: 352.0
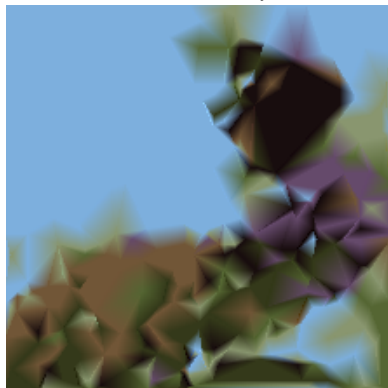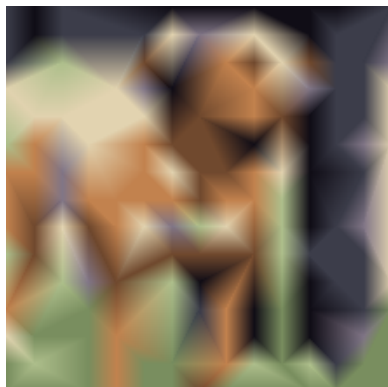

PSNR: 20.30; SSIM: 0.592; bytes: 378.0
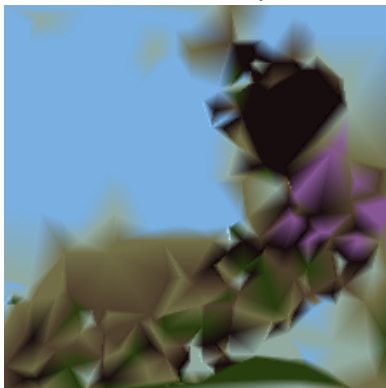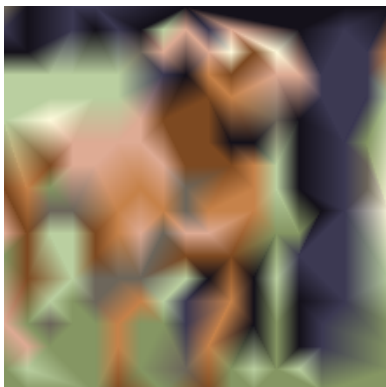

PSNR: 20.39; SSIM: 0.600; bytes: 396.0

PSNR: 20.43; SSIM: 0.600; bytes: 416.0

PSNR: 17.02; SSIM: 0.328; bytes: 102.0

PSNR: 17.39; SSIM: 0.336; bytes: 132.0
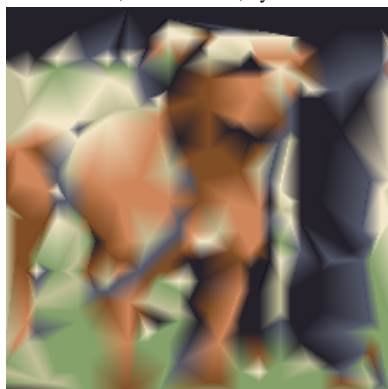
PSNR: 17.77; SSIM: 0.360; bytes: 154.0

PSNR: 18.28; SSIM: 0.387; bytes: 200.0

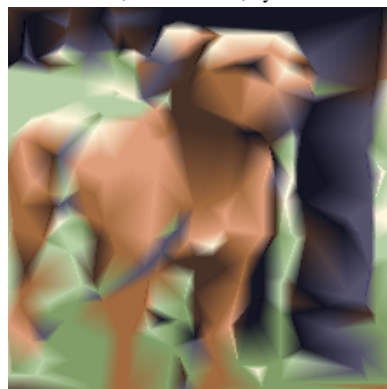PSNR: 18.47; SSIM: 0.395; bytes: 214.0

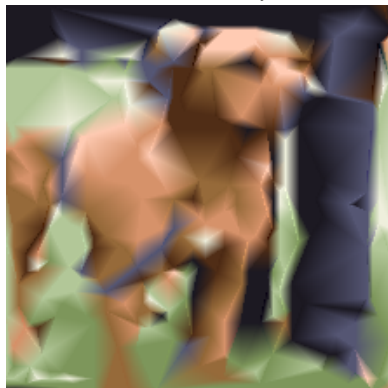PSNR: 18.78; SSIM: 0.405; bytes: 242.0

PSNR: 18.97; SSIM: 0.424; bytes: 284.0

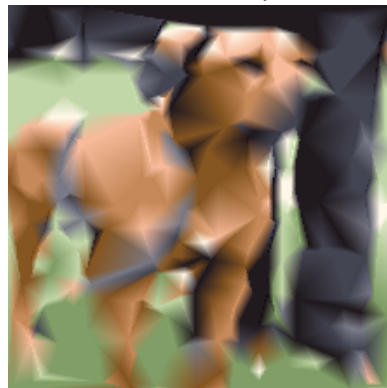PSNR: 19.45; SSIM: 0.452; bytes: 340.0

PSNR: 19.54; SSIM: 0.456; bytes: 388.0

PSNR: 19.83; SSIM: 0.470; bytes: 398.0

PSNR: 19.84; SSIM: 0.470; bytes: 456.0

PSNR: 20.02; SSIM: 0.484; bytes: 472.0